LA-UR-17-26560
Approved for public release; distribution is unlimited.

Title: Mathematical Basis and Test Cases for Colloid-Facilitated Radionuclide Transport Modeling in GDSA-PFLOTRAN

Author(s): Reimus, Paul William

Intended for: Report

Issued: 2017-07-31

# *Mathematical Basis and Test Cases for Colloid-Facilitated Radionuclide Transport Modeling in GDSA-PFLOTRAN*

**Fuel Cycle Research & Development**


***Prepared for***
***U.S. Department of Energy***
***Spent Fuel and Waste Science Technology***
***Paul W. Reimus,***
***Los Alamos National Laboratory***


***August 2017***
**SFWD-SFWST-2017-000117**
**LA-UR-17-XXXXX**

# FCT DOCUMENT COVER SHEET[1]

| | |
|---|---|
| Name/Title of Deliverable/ Milestone/Revision No. | Mathematical Basis and Test Cases for Colloid-Facilitated Radionuclide Transport Modeling in GDSA-PFLOTRAN, M4SF-17LA010504031. Rev 0. |
| Work Package Title & Number | FEPS Analysis – LANL: FT-17LA01050403 (Rev. 2) |
| Work Package WBS Number | **1.08.01.05.04** |
| Responsible Work Package Manager | Paul W. Reimus<br>(Name/Signature) |
| Date Submitted | August 2017 |

| Quality Rigor Level for Deliverable/Milestone[2] | ☐ QRL-1<br>☐ Nuclear Data | ☐ QRL-2 | ☐ QRL-3 | ☒ QRL-4<br>Lab- Specific |
|---|---|---|---|---|

This deliverable was prepared in accordance with Los Alamos National Laboratory
*(Participant/National Laboratory Name)*

QA program which meets the requirements of

☒ DOE Order 414.1 ☐ NQA-1-2000 ☐ Other

**This Deliverable was subjected to:**

☒ Technical Review ☐ Peer Review

**Technical Review (TR)**
**Review Documentation Provided**

☐ Signed TR Report or,

☐ Signed TR Concurrence Sheet or,
Concurrence Sheet or,

☒ Signature of TR Reviewer(s) below
Reviewer(s) below

**Peer Review (PR)**
**Review Documentation Provided**

☐ Signed PR Report or,

☐ Signed PR

☐ Signature of PR

**Name and Signature of Reviewers**

Thomas Corbet

**NOTE 1:** *This sheet should be filled out and submitted with the deliverable. Or, if the PICS:NE system permits, completely enter all applicable information in the PICS:NE Deliverable Form. The requirement is to ensure that all applicable information is entered either in the PICS:NE system or by using the FCT Document Cover Sheet.*

- *In some cases there may be a milestone where an item is being fabricated, maintenance is being performed on a facility, or a document is being issued through a formal document control process where it specifically calls out a formal review of the document. In these cases, documentation (e.g., inspection report, maintenance request, work planning package documentation or the documented review of the issued document through the document control process) of the completion of the activity, along with the Document Cover Sheet, is sufficient to demonstrate achieving the milestone.*

**NOTE 2**: *If QRL 1, 2, or 3 is not assigned, then the QRL 4 box must be checked, and the work is understood to be performed using laboratory specific QA requirements. This includes any deliverable developed in conformance with the respective National Laboratory / Participant, DOE or NNSA-approved QA Program.*

This page left blank intentionally.

# CONTENTS

# FIGURES

# TABLES

No Tables

# MATHEMATICAL BASIS AND TEST CASES FOR COLLOID-FACILITATED RADIONUCLIDE TRANPSORT MODELING IN GDSA-PLOTRAN

## EXECUTIVE SUMMARY

This report provides documentation of the mathematical basis for a colloid-facilitated radionuclide transport modeling capability that can be incorporated into GDSA-PFLOTRAN. It also provides numerous test cases against which the modeling capability can be benchmarked once the model is implemented numerically in GDSA-PFLOTRAN. The test cases were run using a 1-D numerical model developed by the author, and the inputs and outputs from the 1-D model are provided in an electronic spreadsheet supplement to this report so that all cases can be reproduced in GDSA-PFLOTRAN, and the outputs can be directly compared with the 1-D model. The cases include examples of all potential scenarios in which colloid-facilitated transport could result in the accelerated transport of a radionuclide relative to its transport in the absence of colloids. Although it cannot be claimed that all the model features that are described in the mathematical basis were rigorously exercised in the test cases, the goal was to test the features that matter the most for colloid-facilitated transport; i.e., slow desorption of radionuclides from colloids, slow filtration of colloids, and equilibrium radionuclide partitioning to colloids that is strongly favored over partitioning to immobile surfaces, resulting in a substantial fraction of radionuclide mass being associated with mobile colloids.

# 1. INTRODUCTION

Colloid-facilitated transport is generally considered to be the most likely mechanism for transport of low-solubility and/or strongly adsorbing radionuclides over significant distances in groundwater in the geosphere. In the absence of colloids or very strong complexing agents (typically anions that form stable neutral or negatively-charged complexes with nuclides), such radionuclides will be predicted to migrate only very short distances in natural systems over time scales of concern because of their extremely strong interactions with geomedia surfaces (either as adsorbed species or surface precipitates). Thus, it is important that that the General Disposal System Analysis - PFLOTRAN model (GDSA-PFLOTRAN) that is being developed to support nuclear waste repository performance assessments in the Spent Fuel and Waste Systems Technology (SFWST) Campaign be capable of efficiently simulating colloid-facilitated radionuclide transport.

In August 2016, the SFWST Campaign (then called the Used Fuel Disposition Campaign) produced the report "Colloid-Facilitated Radionuclide Transport: Current State of Knowledge from a Nuclear Waste Repository Risk Assessment Perspective" (Reimus et al., 2016) in which a mathematical model was presented and a 1-D numerical version of the model was exercised to illustrate different types of colloid-facilitated radionuclide transport behavior that could have an impact on nuclear waste repository performance assessments. The purpose of the current report is to provide full documentation of the mathematical basis of the model presented in Reimus et al. (2016) and also to provide documentation of inputs and outputs of selected cases that were described in that report so that they can serve as benchmark test cases for the GDSA-PFLOTRAN model. The numerical model used for the current report (and in Reimus et al., 2016) was written in FORTRAN by the author, and although there have been no rigorous efforts to verify or validate it, it has been used successfully to interpret several different laboratory and field-scale transport experiments involving colloid-facilitated radionuclide transport. The model effectively represents all the relevant processes that have been observed in the experiments, although it does not necessarily reflect all the mechanistic details of the processes, many of which remain unknown. The experiment interpretations are described in Reimus et al. (2016) and are not repeated in the current report.

Chapter 2 of this report provides a mathematical description of the model with sufficient clarity to allow a GDSA-PFLOTRAN developer to replicate the workings of the model in the PFLOTRAN framework. Chapter 3 provides documentation of several test cases of the 1-D numerical model that can be used to benchmark the GDSA-PFLOTRAN model. Although agreement between the models does not necessarily constitute a "validation" of the either model, it can serve as a verification that the colloid-facilitated radionuclide transport capabilities from the 1-D model have been properly implemented in GDSA-PFLOTRAN. Furthermore, since the 1-D model has been used to successfully interpret several experimental data sets that have yielded widely varying results, it can be considered a state-of-the-art colloid-facilitated radionuclide transport modeling capability. Of course, comparisons between the two models are limited to 1-D cases in GDSA-PFLOTRAN, but this is justified because all of the key features of the colloid-facilitated radionuclide transport model involve reactive transport processes that overlay nonreactive transport processes (i.e., advection, dispersion, diffusion). It is assumed that nonreactive transport capabilities have been properly implemented in GDSA-PFLOTRAN and that if the reactive transport features associated with colloid-facilitated radionuclide transport are incorporated successfully into 1-D cases, it can be assumed they will be incorporated successfully into multidimensional cases. For simplicity, all of the test cases also involve only a single type of colloid and a single radionuclide solute species, with a similar assumption that if the transport of a single colloid and radionuclide solute species are properly depicted in GDSA-PFLOTRAN, the transport of multiple types of colloids and multiple radionuclides should also be properly depicted in the model. Other simplifying assumptions in the benchmarking test cases are discussed in appropriate places in Chapters 2 and 3.

# 2. COLLOID-FACILITATED RADIONUCLIDE TRANSPORT MODEL MATHEMATICAL BASIS

A generalized mathematical model for colloid-facilitated radionuclide transport, written for flow in parallel-plate fractures with diffusion into a surrounding matrix (y-direction), which represents non-flowing or secondary porosity, is provided below. Note that colloid diffusion into secondary porosity is assumed to be negligible, so there are no equations for colloids in the secondary porosity. The model equations also apply equally well to a porous medium if the matrix or secondary porosity is set equal to zero and the fracture properties are taken to be the porous medium properties (in this case, all equations for transport in the matrix can be ignored).

The equations are written for only a single type of colloid and a single radionuclide solute species, but in general there could be an entire population of colloids having different properties and a number of solute species that may not only interact with surfaces and colloids but could also potentially interact with each other. A separate set of equations must be written for each separate colloid or solute, and additional terms must be added to the solute transport equations if there are multiple types of colloids that the solutes can interact with or if the solutes can interact with each other. Spatially-varying properties/parameters can be assumed, but these are not specified here. We allow for the possibility of multiple solute adsorption sites on both the colloids and immobile surfaces in the system because this feature is rather important for explaining the observed colloid-facilitated transport behavior in many experimental systems. We also allow for multiple colloid filtration sites on immobile surfaces in the system, although only one reversible and one irreversible colloid filtration site have been sufficient to explain all experimental data sets that have been analyzed to date (both lab and field).

Mobile Colloid Transport, Generation and Filtration in Fractures:

In general:

$$\frac{\partial C_c}{\partial t} + div(v_c C_c - D_c \nabla C_c) = \sum_{i=1}^{nfiltsites} \left[ -k_{cs,i} \frac{SA}{V} C_c \left(1 - \frac{S_{c,i}}{S_{c.max,i}}\right) + k_{sc,i} \frac{SA}{V} S_{c,i} \right] + \frac{SA}{V} P_c \qquad (2\text{-}1)$$

Filtered/Immobilized Colloids in Fractures (*nfiltsites* equations):

$$\frac{\partial S_{c,i}}{\partial t} = k_{cs,i} C_c \left(1 - \frac{S_{c,i}}{S_{c,max,i}}\right) - k_{sc,i} S_{c,i} \qquad (2\text{-}2)$$

Mobile Solute in Fractures:

*Advective and Dispersive Transport:* $\frac{\partial C_a}{\partial t} + div(v_a C_a - D_a \nabla C_a) =$

*Reactions with Immobile Surfaces:* $\sum_{i=1}^{nsites} \left[ -k_{as,i} \frac{\rho_B}{\emptyset} C_a \left(1 - \frac{S_{a,i}}{S_{a,max,i}}\right) + k_{sa,i} \frac{\rho_B}{\emptyset} S_{a,i} \right] +$

*Reactions with Mobile Colloids:* $\sum_{i=1}^{ncolsites} \left[ -k_{ac,i} C_a C_c \left(1 - \frac{C_{ac,i} C_c}{C_{ac,max,i} C_c}\right) + k_{ca,i} C_{ac,i} C_c \right] +$

*Reactions with Immobile Colloids:* $\sum_{i=1}^{ncolsites} \left[ \sum_{j=1}^{nfiltsites} \frac{SA}{V} \left[ -k_{ac,i} C_a S_{c,j} \left(1 - \frac{C_{ac,i} S_{c,j}}{C_{ac,max,i} S_{c.j}}\right) + k_{ca,i} C_{ac,i} S_{c,j} \right] \right]$

*Diffusion in and out of Matrix:* $-\frac{\emptyset_m D_{ma}}{b\emptyset} \frac{\partial C_a}{\partial y}\Big|_{y=b}$ (2-3)

Solute Adsorbed onto Immobile Surfaces in Fractures (*nsites* equations):

$$\frac{\partial S_{a,i}}{\partial t} = k_{as,i} C_a \left(1 - \frac{S_{a,i}}{S_{a,max,i}}\right) - k_{sa,i} S_{a,i} \tag{2-4}$$

Solute Adsorbed onto Mobile Colloids in Fractures (ncolsites equations):

$$\frac{\partial C_{ac,i} C_c}{\partial t} + div\left(v_a C_{ac,i} C_c - D_c \nabla C_{ac,i} C_c\right) = k_{ac,i} C_{ac,i} C_c \left(1 - \frac{C_{ac,i} C_c}{C_{ac,max,i} C_c}\right) - k_{ca,i} C_{ac,i} C_c +$$
$$\sum_{j=1}^{nfiltsites} \left[-k_{cs,j} \frac{SA}{V} C_{ac,i} C_c \left(1 - \frac{S_{c,j}}{S_{c,max,j}}\right) + k_{sc,j} \frac{SA}{V} C_{ac,i} S_{c,j}\right] \tag{2-5}$$

Solute Adsorbed onto Immobile Colloids in Fractures (*ncolsites* x *nfiltsites* equations):

$$\frac{\partial C_{ac,i} S_{c,j}}{\partial t} = k_{ac,i} C_a S_{c,j} \left(1 - \frac{C_{ac,i} S_{c,j}}{C_{ac,max,i} S_{c,j}}\right) - k_{ca,i} C_{ac,i} S_{c,j} +$$
$$k_{cs,j} C_{ac,i} C_c \left(1 - \frac{C_{ac,i} S_{c,j}}{C_{ac.i} S_{c,max,j}}\right) - k_{sc.j} C_{ac,i} S_{c,j} \tag{2-6}$$

Solute Diffusion and Reaction in Matrix (no Colloids assumed in Matrix):

$$\frac{\partial C_a}{\partial t} - D_{ma} \frac{\partial^2 C_a}{\partial y^2} = \sum_{i=1}^{nmatrixsites} \left[-k_{am,i} \frac{\rho_{Bm}}{\emptyset_m} C_a \left(1 - \frac{S_{am,i}}{S_{am,max,i}}\right) + k_{ma,i} \frac{\rho_{Bm}}{\emptyset_m} S_{am,i}\right] \tag{2-7}$$

Solute Adsorbed to Immobile Surfaces in Matrix (*nmatrixsites* equations):

$$\frac{\partial S_{am,i}}{\partial t} = k_{am,i} C_a \left(1 - \frac{S_{am,i}}{S_{am,max,i}}\right) - k_{ma,i} S_{am,i} \tag{2-8}$$

where, $C_c$ = concentration of colloids in mobile phase, g/cm$^3$
$S_{c,i}$ or $S_{c,j}$ = colloid concentration on filtration site *i* or *j* on fracture surfaces, g/cm$^2$
$S_{c.max,i}$ or $S_{c.max,j}$ = maximum colloid concentration on filtration site *i* or *j* on fracture surfaces, g/cm$^2$
$C_a$ = solution concentration of solute in fractures or matrix, g/cm$^3$
$S_{a,i}$ = adsorbed concentration of solute on fracture surface site *i*, g/g
$S_{am,i}$ = adsorbed concentration of solute on matrix surface site *i*, g/g
$C_{ac,i}$ = concentration of solute sorbed to colloid site *i*, g/g colloid
$S_{a,max,i}$ = maximum adsorbed concentration of solute on fracture surface site *i*, g/g
$S_{am,max,i}$ = maximum adsorbed concentration of solute on matrix surface site *i*, g/g
$C_{ac,max,i}$ = maximum concentration of solute sorbed to colloid site *i*, g/g colloid
$P_c$ = colloid production rate in fractures, g/cm$^2$-hr
$v_c$ = advective velocity of colloids in fractures, cm/hr
$v_a$ = advective velocity of solutes in fractures, cm/hr
$D_a$ = solute dispersion coefficient in fractures, cm$^2$/hr
$D_c$ = colloid dispersion coefficient in fractures, cm$^2$/hr
$D_{ma}$ = solute molecular diffusion coefficient in matrix, cm$^2$/hr
$\rho_B$ = effective bulk density within fractures, g/cm$^3$
$\rho_{Bm}$ = bulk density in matrix, g/cm$^3$.
$\emptyset$ = porosity within fractures
$\emptyset_m$ = matrix porosity
$b$ = fracture half aperture, cm
$\frac{SA}{V}$ = surface area to volume ratio in fractures, cm$^2$/cm$^3$
$k_{cs,i}$ or $k_{cs,j}$ = colloid filtration rate constant for filtration site *i* or *j*, cm$^3$/cm$^2$-hr
$k_{sc,i}$ or $k_{sc,j}$ = reverse colloid filtration (detachment) rate constant for filtration site *i* or *j*, 1/hr
$k_{as,i}$ = rate constant for sorption of solute onto fracture surface site *i*, cm$^3$/g-hr

$k_{sa,i}$ = rate constant for desorption of solute from fracture surface site *i*, 1/hr
$k_{am,i}$ = rate constant for sorption of solute onto matrix surface site *i*, $cm^3$/g-hr
$k_{ma,i}$ = rate constant for desorption of solute from matrix surface site *i*, 1/hr
$k_{ac,i}$ = rate constant for sorption of solute onto colloid site *i*, $cm^3$/g-hr
$k_{ca,i}$ = rate constant for desorption of solute from colloid site *i*, 1/hr
*nfiltsites* = number of different types of filtration sites for colloids on fracture surfaces
*nsites* = number of different types of adsorption sites for solutes on fracture surfaces
*ncolsites* = number of different types of adsorption sites for solutes on colloid surfaces
*nmatrixsites* = number of different types of adsorption sites for solutes on matrix surfaces

Equations (2-1) through (2-8) are provided for completeness so that a colloid-facilitated transport modeling capability with maximum flexibility can be incorporated into GDSA-PFLOTRAN. Note that equations (2-1) and (2-3) are written with grad and divergence expressions to describe advective and dispersive transport in up to 3 dimensions. However, in the remainder of this report, the test cases will be restricted to one dimensional advective and dispersive transport to accommodate the numerical model developed by the author. It is also noteworthy that the reactions between colloids and immobile surfaces, solutes and immobile surfaces, and solutes and colloids are all described by first-order reactions with an adsorption site capacity that limits how much solute can be adsorbed onto either colloids or immobile surfaces or how much colloids can be attached to immobile surfaces. The use of first-order rate expressions does not mean that equilibria between phases cannot be represented; it means it must be represented by using rapid forward and reverse reaction rates relative to transport rates and treating the ratio of the forward to reverse reaction rates as effective equilibrium partition coefficients. Of course, equilibrium expressions could be incorporated directly into GDSA-PFLOTRAN as appropriate.

# 3. BENCHMARKING TEST CASES FOR GDSA-PFLOTRAN

For the benchmarking test cases, the model of equations (2-1) through (2-8) is simplified by reducing the number of different types of radionuclide adsorption sites on both colloids and immobile surfaces to one each (*nsites* = *ncolsites* = 1), and also secondary porosity is assumed to be zero ($\emptyset_{\boldsymbol{m}}$ = 0, so there are no matrix transport equations). We also assume (except for one final test case described in Section 3.5) that colloids undergo only irreversible filtration with a single type of filtration site (*nfiltsites* = 1 and $k_{sc,1} = k_{sc}$ = 0), and we further assume that there are effectively no sorption or filtration site capacity limitations ($S_{max}$ values are very large) for solute sorption reactions onto fracture or colloid surfaces and also for colloid filtration onto fracture surfaces. These simplifications and assumptions allow us to reduce equations (2-1) to (2-8) to the following six 1-D transport equations, none of which contain summation terms, $S_{max}$ terms, or *i* or *j* subscripts to denote different types of sites (and we now refer to a flow domain instead of fractures and immobile surfaces instead of fracture surfaces because the fracture designation is no longer relevant):

Mobile and Immobile Colloids in Flow Domain:

$$\frac{\partial C_c}{\partial t} + v_c \frac{\partial C_c}{\partial x} - D_c \frac{\partial^2 C_c}{\partial x^2} = -k_{cs,ir} \frac{SA}{V} C_c + \frac{SA}{V} P_c \tag{3-1}$$

$$\frac{\partial S_{c,ir}}{\partial t} = k_{cs,ir} C_c \tag{3-2}$$

Mobile and Immobile Solute in Flow Domain:

$$\frac{\partial C_a}{\partial t} + v_a \frac{\partial C_a}{\partial x} - D_a \frac{\partial^2 C_a}{\partial x^2} = -k_{as} \frac{\rho_B}{\emptyset} C_a + k_{sa} \frac{\rho_B}{\emptyset} S_a - k_{ac} C_a C_c + k_{ca} C_{ac} C_c - k_{ac} C_a S_{c,ir} + k_{ca} C_{ac} S_{c,ir} \tag{3-3}$$

$$\frac{\partial S_a}{\partial t} = k_{as} C_a - k_{sa} S_a \tag{3-4}$$

Solute Adsorbed onto Mobile Colloids in Flow Domain:

$$\frac{\partial C_{ac} C_c}{\partial t} + v_c \frac{\partial C_{ac} C_c}{\partial x} - D_c \frac{\partial^2 C_{ac} C_c}{\partial x^2} = k_{ac} C_{ac} C_c - k_{ca} C_{ac} C_c - k_{cs,ir} \frac{SA}{V} C_{ac} C_c \tag{3-5}$$

Solute Adsorbed onto Immobile Colloids in Flow Domain:

$$\frac{\partial C_{ac} S_{c,ir}}{\partial t} = k_{ac} C_a S_{c,ir} - k_{ca} C_{ac} S_{c,ir} + k_{cs,ir} C_{ac} C_c \tag{3-6}$$

where, $S_{c,ir}$ = colloid concentration on irreversible filtration sites on fracture surfaces, g/cm$^2$
$S_{c,max,ir}$ = maximum colloid concentration on irreversible filtration sites on fracture surfaces, g/cm$^2$
$k_{cs,ir}$ = irreversible colloid filtration rate constant, cm$^3$/cm$^2$-hr

Before discussing the test cases further, we note that if we are dealing with a system where natural colloid concentrations are constant throughout the flow domain and there are no colloids being generated at the source, equations (3-1) and (3-2) can effectively be dropped from consideration and simply replaced with a constant colloid concentration, $C_c$, everywhere in the system. Furthermore, if solute reactions with immobile surfaces and colloids are fast relative to time scales of transport (both adsorption and desorption rates), then these reactions can be considered to be at equilibrium, and the rate expressions can be replaced with partition coefficient expressions in a single equation describing solute transport through the flow system. These simplifications allow equations (3-1) to (3-6) to be reduced to a single equation:

$$\frac{\partial C_a}{\partial t} + v_a \frac{\partial C_a}{\partial x} - D_a \frac{\partial^2 C_a}{\partial x^2} + \frac{\rho_B}{\emptyset} K_d \frac{\partial C_a}{\partial t} + K_c C_c \frac{\partial C_a}{\partial t} + K_c C_c \left( v_c \frac{\partial C_a}{\partial x} - D_c \frac{\partial^2 C_a}{\partial x^2} \right) = 0 \tag{3-7}$$

where, $K_d = k_{as}/k_{sa}$ = partition coefficient for solute on immobile surfaces, cm$^3$/g
$K_c = k_{ac}/k_{ca}$ = partition coefficient for solute on colloids, cm$^3$/g

$C_{ac} = K_c C_c C_a$, and
$C_{as} = K_d C_a$

If $v_a = v_c$ (solute and colloid velocities are equal) and $D_a = D_c$ (solute and colloid dispersion coefficients are equal), then equation (3-7) can be rearranged to yield:

$$\left(1 + \frac{\rho_B}{\emptyset} K_d + K_c C_c\right) \frac{\partial C_a}{\partial t} + (1 + K_c C_c) \left(v_a \frac{\partial C_a}{\partial x} - D_a \frac{\partial^2 C_a}{\partial x^2}\right) = 0 \quad (3\text{-}8)$$

or alternatively,

$$\left(\frac{1 + \frac{\rho_B}{\emptyset} K_d + K_c C_c}{1 + K_c C_c}\right) \frac{\partial C_a}{\partial t} \frac{\rho_B}{\emptyset} + v_a \frac{\partial C_a}{\partial x} - D_a \frac{\partial^2 C_a}{\partial x^2} = 0 \quad (3\text{-}9)$$

from which it is readily apparent that the term, $\frac{\mathbf{1 + \frac{\rho_B}{\emptyset} K_d + K_c C_c}}{\mathbf{1 + K_c C_c}}$, is an effective retardation factor for solute transport through the system. We do not explicitly use equations (3-7) through (3-9) in any of the test cases, but some of the test cases have inputs that make these equations applicable; and thus the effective retardation factor expression can be used to verify the test cases.

All of the test cases assume a steady input of both colloids and radionuclides at the entrance to the domain starting at time zero (i.e., a step function input, rather than a pulse). Such an input function is reasonable for a breached repository, which will presumably release colloids and radionuclides indefinitely once it is compromised. We also assume steady-state flow with a fixed dispersion coefficient for both colloids and solutes, and no spatial variability of any model parameters within the model domain. In all cases, a dimensionless dispersion coefficient, $D_a/vL$, of 0.02 is assumed, which is equivalent to a Peclet number, $vL/D_a$, of 50. We also assume that solute adsorption to and desorption from the immobile surfaces is rapid and relatively strong, with $\frac{\rho_B}{\emptyset} \frac{k_{as}}{k_{sa}} = \frac{\rho_B}{\emptyset} K_d$ = 1000 (dimensionless). This assumption results in a solute retardation factor of 1001 in the absence of colloids, meaning that the breakthrough of the reactive solute is approximately 1000 times later than the breakthrough of a nonreactive species.

In the remainder of this chapter, we present the results of a series of 1-D finite-difference numerical model simulations that can be used as benchmarking cases for GDSA-PFLOTRAN. The results of the simulations are presented as radionuclide breakthrough curves in which the dimensionless radionuclide concentration ($C/C_0$, where $C_0$ is the input concentration) is plotted vs. dimensionless time ($t/\tau$, where $\tau$ is the mean groundwater residence time in the flow system). The mean groundwater residence time is equal to $L/v$, with $L$ being the length of the flow domain and $v$ the average velocity through the domain. The breakthrough curves are presented as being associated with different values of dimensionless rate constants (effective rate constants multiplied by $\tau$) or, when equations (3-7) to (3-9) apply, different values of the effective retardation factor, $\frac{\mathbf{1 + K_d \frac{\rho_B}{\emptyset} + K_c C_c}}{\mathbf{1 + K_c C_c}}$. However, all of the 1-D model inputs and outputs for each test case are listed in an electronic spreadsheet supplement to this report so that the exact dimensional inputs can be replicated in GDSA-PFLOTRAN, and likewise the GDSA-PFLOTRAN outputs can be compared to dimensional outputs from the 1-D model.

## 3.1 First Set of Test Cases: Early Breakthrough of Small Radionuclide Mass Fraction Associated with Pseudocolloids

We first consider a situation where a radionuclide is released as a solute at the entrance to the flow domain, with no initial association with colloids, but with a strong adsorption affinity to the colloids, which are present at constant concentration throughout the domain. This is equivalent to a scenario where natural colloids (i.e., "pseudocolloids") are assumed to be the colloids that facilitate the transport of the radionuclide. The colloids are assumed to be present at a concentration of 1 mg/L or $10^{-6}$ g/cm$^3$. To achieve

this concentration while still assuming that there is a finite irreversible colloid filtration rate, we must assume that the irreversible filtration of colloids is balanced by a steady colloid production rate. Using the steady-state version of equation (3-1) (i.e., all derivatives set equal to zero), we see that this production rate must be given by:

$$P_c = k_{cs,ir} C_c \tag{3-10}$$

Fig. 3-1 shows the predicted breakthrough curves of colloid-associated radionuclide solute, free solute, and total solute when the solute association with colloids is given by an adsorption rate constant multiplied by $\tau$, $k_{ac}\tau$, = $10^5$ cm$^3$/g colloids, a dimensionless desorption rate constant $k_{ca}\tau$ = 0.1, and a dimensionless

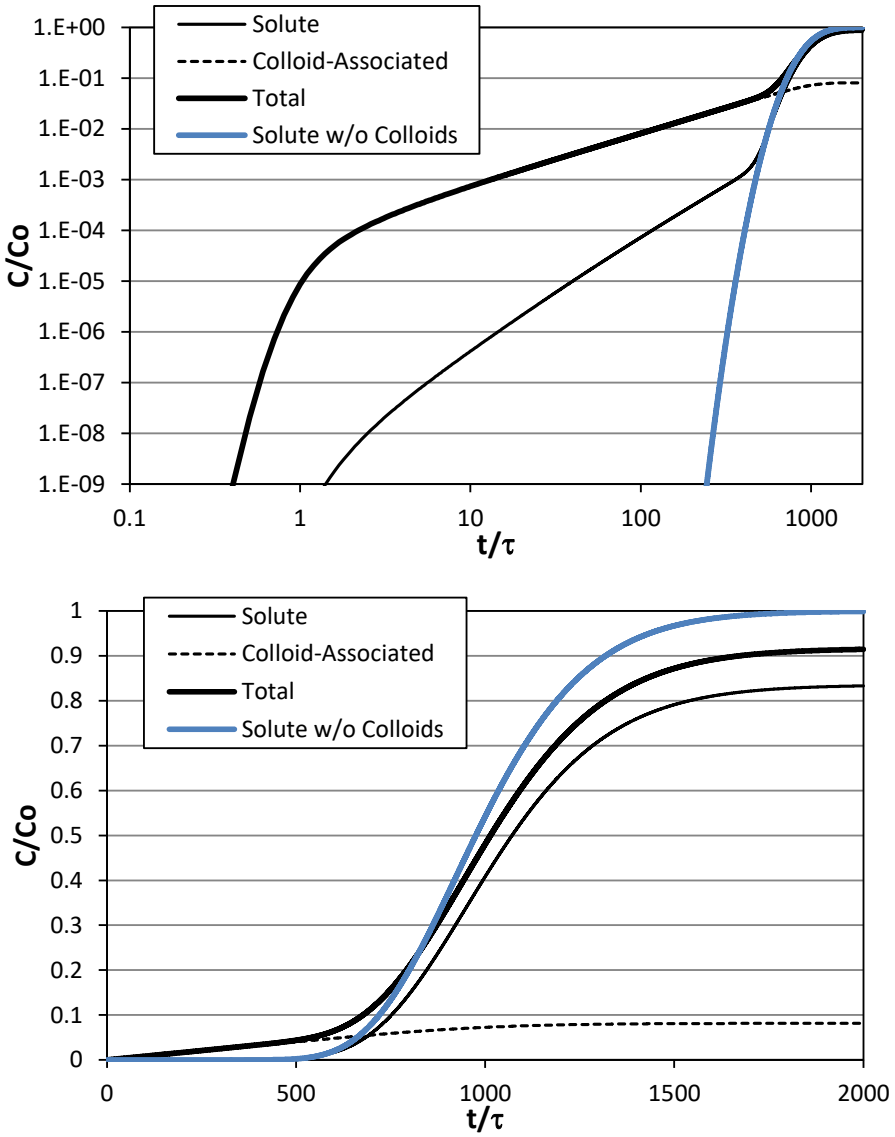


Figure 3-1. Solute, colloid-associated, and total breakthrough curves of a radionuclide assuming the following model parameter values: $k_{ac}\tau$, = $10^5$ cm$^3$/g colloids, $k_{ca}\tau$ = 0.1, $\frac{SA}{V}k_{cs,ir}\tau$ = 0.1, $\frac{\rho_B}{\emptyset}K_d$ =1000, and $C_c$ = $10^{-6}$ g/cm$^3$. The blue curve is the radionuclide breakthrough in the absence of colloids. Upper plot has logarithmic scales for axes, and lower plot has linear scales (same curves in each plot).

colloid filtration rate constant $\frac{SA}{V}k_{cs,ir}\tau$ = 0.1. Note that the upper plot of Fig. 3-1 has log axes whereas the lower plot has linear axes, and in both cases a curve for the radionuclide breakthrough in the absence of colloids is also shown. The input parameters for these cases, including both the colloid-free case and the case with colloids, are provided in the electronic spreadsheet supplement to this report in the worksheet titled "Figure 3-1 Test Cases", and the resulting dimensional output concentrations of species as a function of time from the 1-D model are also provided in this worksheet in a format that can be readily cut-and-pasted into a spreadsheet or other tabular format. The dimensional inputs are listed using the same notation that is provided after equations (2-1) through (2-8), and also after equations (3-1) through (3-6). For additional discussion about the significance and implications of the test cases, the reader is referred to Reimus et al., (2016), Section 2.1.

Fig. 3-2 shows the breakthrough curves for cases in which $k_{ca}\tau$ is kept at a value of 0.1, but $\frac{SA}{V}k_{cs,ir}\tau$ is increased to 1 and 10. It is clear that the increase in colloid irreversible filtration rate constant results in significantly lower early breakthroughs of radionuclides associated with colloids. If the irreversible filtration rate constant is increased much beyond the larger value, the early breakthrough of solute (relative to the colloid-free case) will disappear altogether. These two cases serve as examples of a significant amount and a muted amount of early solute breakthrough mass fractions, respectively. The input parameters and 1-D model outputs for these cases, are provided in the electronic spreadsheet supplement to this report in the worksheet titled "Figure 3-2 Test Cases".

Fig. 3-3 shows two sets of breakthrough curves where the value of $k_{ca}\tau$ is 1 (a factor of 10 higher than in the cases of Fig. 3-2), and the values of $\frac{SA}{V}k_{cs,ir}\tau$ are, respectively, 1 and 10. The early breakthroughs of solute are slightly lower and the late breakthroughs are considerably higher in Fig. 3-3 than in Fig. 3-2 because the radionuclide is desorbing ten times faster from the colloids in Fig. 3-3. This more rapid desorption rate reduces the concentration of solute that breaks through early because less solute mass remains adsorbed to the rapidly-transporting colloids, but it increases the late breakthrough concentrations because the solute more rapidly desorbs from irreversibly-filtered colloids at late times, thus contributing to a higher late concentration. The input parameters and 1-D model outputs for these cases, are provided in the electronic spreadsheet supplement to this report in the worksheet titled "Figure 3-3 Test Cases".

Fig. 3-4 is analogous to Fig. 3-3 except that in this case the series of breakthrough curves correspond to a fixed value of $\frac{SA}{V}k_{cs,ir}\tau$ = 1 and varying values of $k_{ca}\tau$ (1 and 10). The values of $[\exp(-k_{ca}\tau)][\exp(-\frac{SA}{V}k_{cs,ir}\tau)]$ for the curves in the two figures are the same, and, as discussed in Reimus et al. (2016), it is apparent that the early breakthroughs are essentially identical, which underscores that it is the product of these two exponential expressions that defines the magnitude of the early breakthroughs, not the individual values of either $\frac{SA}{V}k_{cs,ir}\tau$ or $k_{ca}\tau$. The input parameters and 1-D model outputs for these cases, are provided in the electronic spreadsheet supplement to this report in the worksheet titled "Figure 3-4 Test Cases".

Fig. 3-5 shows the impact of increasing the rate constant for radionuclide adsorption to the colloids, $k_{ac}$, by one order of magnitude for $\frac{SA}{V}k_{cs,ir}\tau$ values of 1 and 10 while keeping the value of $k_{ca}\tau$ constant at 1. If the curves of Fig. 3-5 are compared with those of Fig. 3-3, it is apparent that the early breakthrough of the radionuclide is about one order of magnitude higher in concentration than in Fig. 3-3 for the same values of $\frac{SA}{V}k_{cs,ir}\tau$, but the shapes of the curves are otherwise very similar. This occurs because the value of $\frac{k_{ac}C_c\tau}{1+k_{ac}C_c\tau+\frac{\rho_B}{\emptyset}K_d}$, which dictates the concentration of the early breakthrough (Reimus et al., 2016), is one order of magnitude higher in Fig. 3-5 than in Fig. 3-3 ($10^{-3}$ vs. $10^{-4}$). The input parameters and 1-D model outputs for the cases of Figure 3-5, are provided in the electronic spreadsheet supplement to this report in the worksheet titled "Figure 3-5 Test Cases".

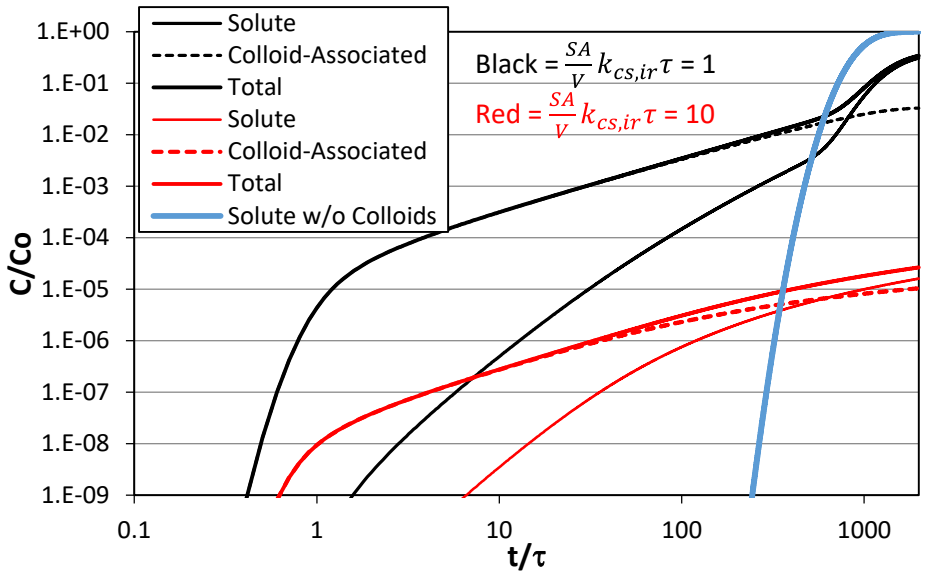


Figure 3-2. Solute, colloid-associated, and total breakthrough curves of a radionuclide assuming the same model parameters as Fig. 3-1 except with $\frac{SA}{V}k_{cs,ir}\tau$ = 1 (black) and 10 (red).

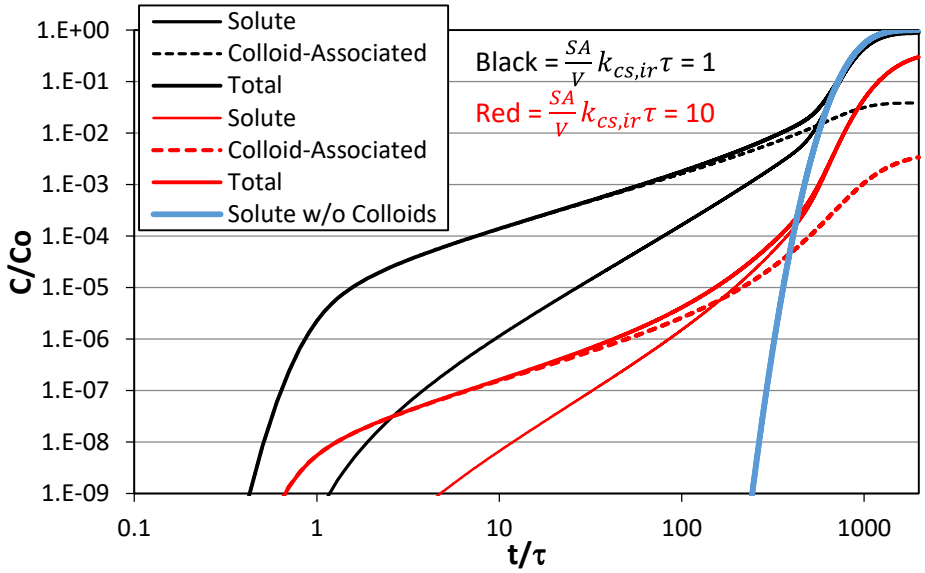


Figure 3-3. Solute, colloid-associated, and total breakthrough curves of a radionuclide assuming $k_{ca}\tau$ is 1 (a factor of 10 higher than in Figs. 3-1 and 3-2) and other parameters are the same as in Figs. 3-1 and 3-2. Values of $\frac{SA}{V}k_{cs,ir}\tau$ are 1 (black) and 10 (red).

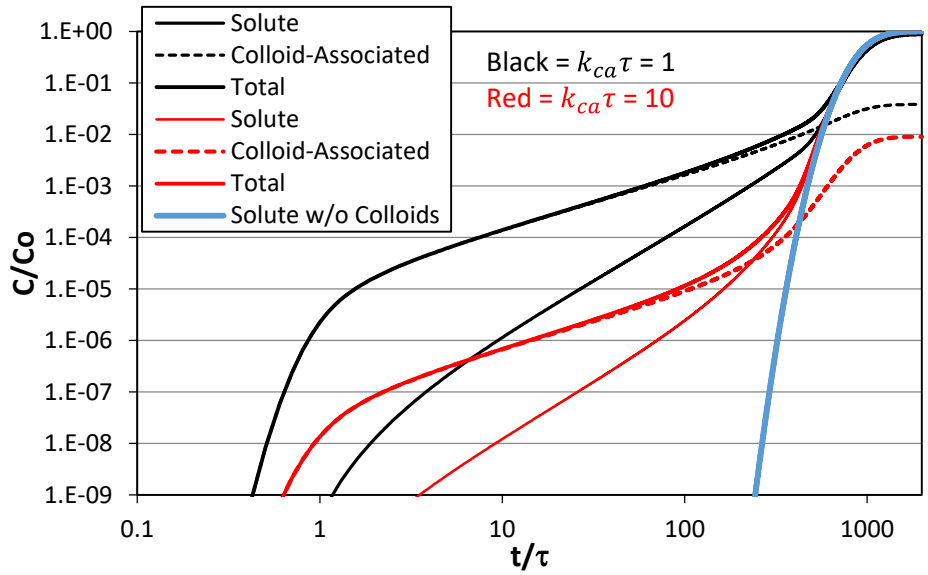


Figure 3-4. Solute, colloid-associated, and total breakthrough curves of a radionuclide assuming $\frac{SA}{V}k_{cs,ir}\tau$ is 1 (a factor of 10 higher than in Fig. 3-1) and the values of $k_{ca}\tau$ are 1 (black) and 10 (red). Other model parameters are same as in Fig. 3-1.

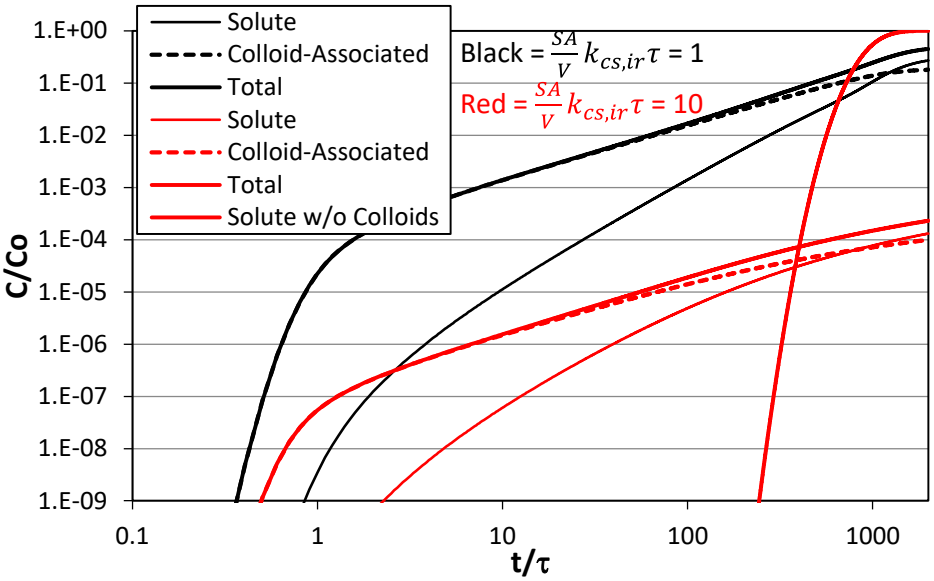


Figure 3-5. Solute, colloid-associated, and total breakthrough curves of a radionuclide assuming $k_{ac}\tau$ is $10^6$ cm$^3$/g colloids (a factor of 10 higher than in all previous figures). Values of $\frac{SA}{V}k_{cs,ir}\tau$ are 1 (black) and 10 (red). Values of all other parameters are the same as in Fig. 3-3.

We note that the results of Fig. 3-5 can be reproduced almost exactly if all adsorption and desorption rate constants are kept the same as in Fig. 3-3, but the steady-state colloid concentrations are increased by an order of magnitude by increasing the steady production rate of colloids while keeping the values of $\frac{SA}{V}k_{fc,ir}\tau$ equal to 1 and 10. Increasing the steady-state colloid concentration has exactly the same effect

as increasing the radionuclide adsorption rate constant onto the colloids because it is the product of these two parameters that appears in the expression defining the initial fraction of radionuclides associated with colloids, i.e., $\frac{k_{ac}C_c\tau}{1+k_{ac}C_c\tau+\frac{\rho_B}{\emptyset}K_d}$. We do not show the results of increasing the steady-state colloid concentrations by an order of magnitude because the curves are identical to Fig. 2-5 (other than minor changes at late times because more filtered colloids become associated with the immobile surfaces when colloid concentrations are higher, and these colloids exert a small influence on the late-time breakthrough by increasing the radionuclide retardation on the immobile surfaces). However, these cases are considered to be good benchmarking test cases for GDSA-PFLOTRAN, so input parameters and 1-D model outputs for them are provided in the electronic spreadsheet supplement to this report in the worksheet titled "Figure 3-5 Test Cases", along with the inputs and outputs for the cases of Fig. 3-5.

## 3.2 Second Set of Test Cases: Early Breakthrough of Small Radionuclide Mass Fraction as Intrinsic Colloids

All of the model results presented and discussed in Section 3.1 consider the radionuclide mass to be released entirely in the solute form and that a small fraction (i.e., approximately $\frac{k_{ac}C_c\tau}{1+k_{ac}C_c\tau+\frac{\rho_B}{\emptyset}K_d}$) becomes rapidly associated with pseudocolloids. We next consider cases where the radionuclide is released entirely in colloidal form, either as an intrinsic colloid or as a waste-form degradation product or corrosion product colloid that has the radionuclide strongly associated with it when generated. In these cases, we assume that the colloidal fraction of the released radionuclide is $10^{-5}$, and that no solute fraction is released, so the early breakthrough concentration can never exceed $10^{-5}$. All other model parameters are the same as in the cases presented in Figs. 3-1 through 3-5, except that there is no production of colloids; i.e., $P_c = 0$ and the initial concentration of intrinsic colloids (carrying radionuclides) in the flow domain is zero. Additional discussion of the cases discussed in this section is provided in Section 2.2 of Reimus et al. (2016).

Fig. 3-6 shows the results for a fixed value of $\frac{SA}{V}k_{cs,ir}\tau = 0.1$ (a slow rate of intrinsic colloid filtration) and two different values of $k_{ca}\tau$ (0.1 and 10), representing varying rates of radionuclide dissociation from the colloids. The case with $k_{ca}\tau = 0.1$ is effectively a case in which there is almost no dissociation of the radionuclide from the intrinsic colloid, and the case with $k_{ca}\tau = 10$ is equivalent to a case where the dissociation is nearly complete. Note that the dissociation may not necessarily be desorption, but it could be some other type of geochemical degradation of the colloid itself. The early breakthrough in the case of $k_{ca}\tau = 0.1$ is essentially a steady concentration plateau of approximately $10^{-5}$ at all times, whereas in the case of $k_{ca}\tau = 10$, the early breakthrough is $10^{-5}$ times the product $[\exp(-k_{ca}\tau)][\exp(-\frac{SA}{V}k_{cs,ir}\tau)]$, although the concentration in this case steadily rises until it reaches $10^{-5}$ at later times because the dissociated radionuclde mass transports through the system as a solute with a retardation factor of ~1000. The input parameters and 1-D model outputs for the cases of Figure 3-6 are provided in the electronic spreadsheet supplement to this report in the worksheet titled "Figure 3-6 Test Cases".

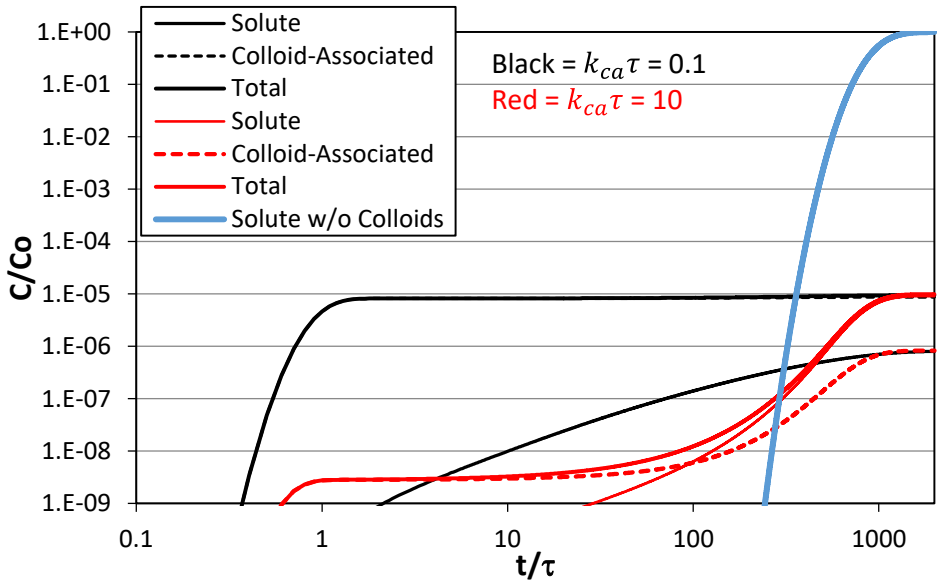


Figure 3-6. Solute, colloid-associated, and total breakthrough curves of a radionuclide assuming a colloidal release fraction of $10^{-5}$, with no solute release fraction. $\frac{SA}{V}k_{cs,ir}\tau$ is 0.1 for all cases. Values of $k_{ca}\tau$ are 0.1 (black) and 10 (red). Other model parameters are same as in Fig. 3-4.

Fig. 3-7 shows results for a fixed value of $k_{ca}\tau$ = 0.1 (a slow rate of radionuclide desorption from colloids) and varying values of $\frac{SA}{V}k_{cs,ir}\tau$ (0.1 and 10, representing varying rates of colloid filtration). It is apparent that these breakthrough curves have essentially the same early breakthroughs as the corresponding cases in Fig. 3-6 that have the same values of the product $[\exp(-k_{ca}\tau)][\exp(-\frac{SA}{V}k_{cs,ir}\tau)]$. However, it is also apparent that the radionuclide breakthrough at late times for the case with $\frac{SA}{V}k_{cs,ir}\tau$ = 10 is significantly lower in Fig. 3-7 than for the case with $k_{ca}\tau$ = 10 in Fig. 3-6. The much greater accumulation of filtered colloids on the immobile surfaces in the case of Fig. 3-7 suppresses the radionuclide breakthroughs at late times because the filtered colloids effectively impart additional retardation capacity to the immobile surfaces. The input parameters and 1-D model outputs for the cases of Figure 3-7 are provided in the electronic spreadsheet supplement to this report in the worksheet titled “Figure 3-7 Test Cases”.

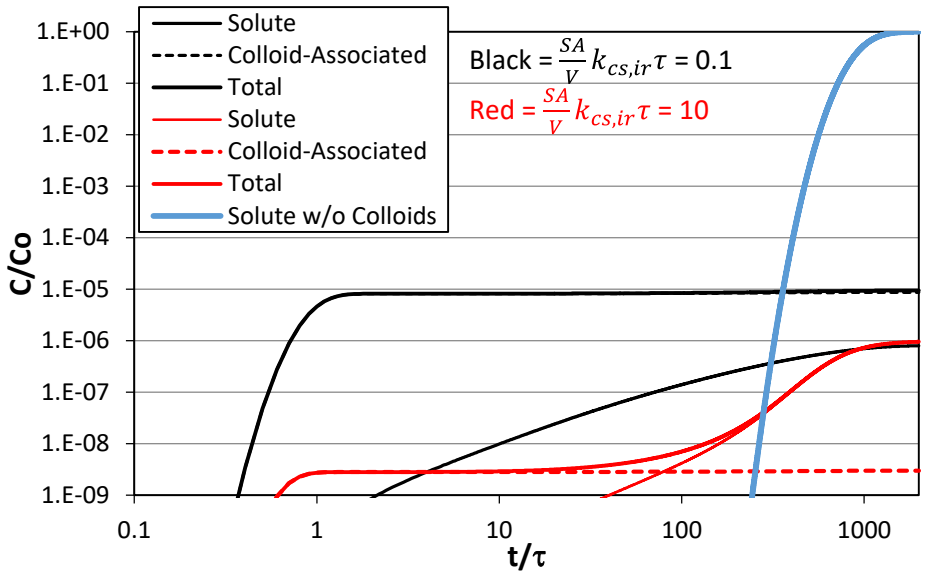


Figure 3-7. Solute, colloid-associated, and total breakthrough curves of a radionuclide assuming a colloidal release fraction of $10^{-5}$, with no solute release fraction. $k_{ca}\tau$ is 0.1 for all cases. Values of $\frac{SA}{V}k_{cs,ir}\tau$ are 0.1 (black) and 10 (red). Other model parameters are same as in Fig. 3-4.

## 3.3 Third Set of Test Cases: Reduced Retardation of a Large Mass Fraction – Strong Equilibrium Partitioning to Pseudocolloids

We next consider cases where the radionuclide adsorption to and desorption from colloids is rapid relative to transport times so that equilibrium partitioning can be assumed for the radionuclide on the colloids as well as on the immobile surfaces. In this case, we revert back to the assumption that the radionuclide is released entirely in the solution phase, and it rapidly partitions between colloids, immobile surfaces and the solution phase. We assume an order of magnitude increase in steady-state colloid concentration, $C_c$, relative to the cases of Figs. 3-1 through 3-5, i.e. 10 mg/L or $10^{-5}$ g/cm$^3$ instead of 1 mg/L or $10^{-6}$ g/cm$^3$. We also assume the same value for $K_c$, or the ratio $k_{ac}/k_{ca}$, as in Figs. 3-1 through 3-4 (i.e., 100,000 ml/g colloid), but the rate constants are increased such that $k_{ca}\tau$ = 100, which is sufficient to approximate equilibrium partitioning to the colloids. All other parameters are kept the same as in the cases of Figs. 3-1 through 3-5. For all of these parameter values, the effective retardation factor expression from equation (3-9), $\frac{1+\frac{\rho_B}{\emptyset}K_d+K_cC_c}{1+K_cC_c}$, is equal to $\frac{1+1000+1}{1+1}$ = 501. Fig. 3-8 shows that the breakthrough of the radionuclide for these parameter values indeed occurs at around $t/\tau$ = 500, which is about a factor of 2 faster than the colloid-free breakthrough at $t/\tau$ = 1000. It can also be shown that the value of $\frac{K_cC_c}{1+K_cC_c}$ is approximately the fraction of breakthrough that is predicted to be associated with colloids whereas the value of $\frac{1}{1+K_cC_c}$ is the fraction of breakthrough predicted to be in the solution phase. Both of these values are 0.5 for the parameter values selected, and Fig. 3-8 shows that the late-time colloid-associated and solute breakthroughs are both indeed $C/C_0$ = 0.5. The input parameters and 1-D model outputs for the cases of Figure 3-8 are provided in the electronic spreadsheet supplement to this report in the worksheet titled "Figure 3-8 Test Case".

Fig. 3-9 shows the results of model calculations where the value of $C_c$ is both increased and decreased by a factor of two relative to Fig. 3-8 while all other parameters are kept the same. The values of $\frac{1+\frac{\rho_B}{\emptyset}K_d+K_cC_c}{1+K_cC_c}$

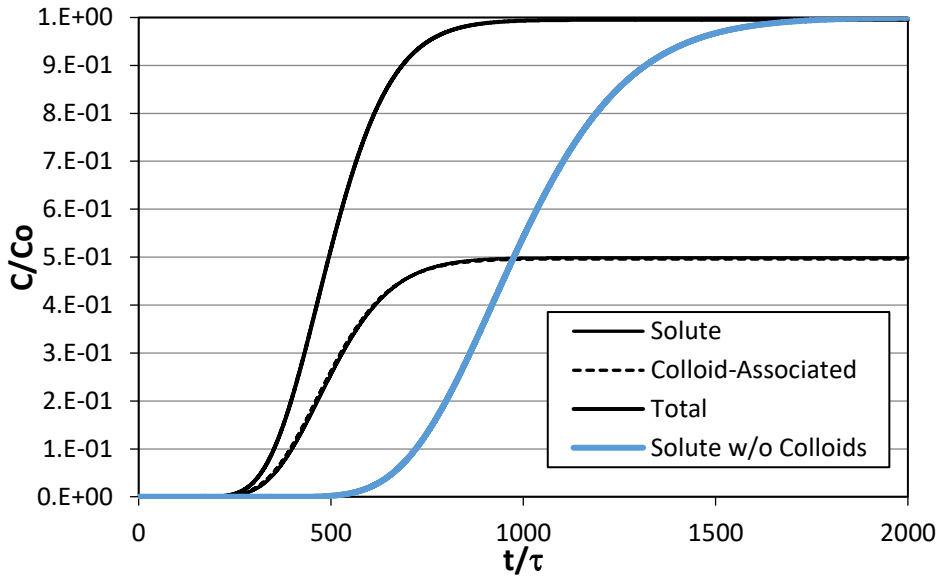


Figure 3-8. Solute, colloid-associated, and total breakthrough curves of a radionuclide assuming $C_c$ = $10^{-5}$ g/cm$^3$, $k_{ac}\tau$, = $10^8$ cm$^3$/g colloids, and $k_{ca}\tau$ = 100. The latter two values have the same ratio of $k_{ac}/k_{ca}$ as in Figs. 3-1 to 3-4, but their values are large enough that equilibrium partitioning between the solute and the colloids can be assumed. The blue curve is the radionuclide breakthrough in the absence of colloids.

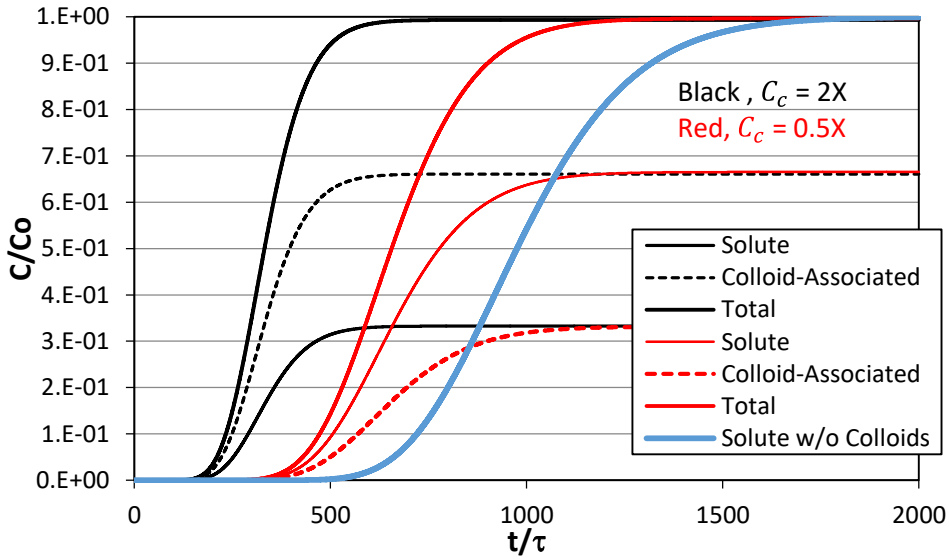


Figure 3-9. Solute, colloid-associated, and total breakthrough curves of a radionuclide assuming the same model parameters as in Fig. 3-8 except that $C_c$ = 2 x $10^{-5}$ g/cm$^3$, or 2 times the value of $C_c$ in Fig. 3-8 (black) and $C_c$ = 5 x $10^{-6}$ g/cm$^3$, or half the value of $C_c$ in Fig. 3-8 (red).

for these two cases are 334 and 668 and the colloid-associated fractions $\frac{K_c C_c}{1+K_c C_c}$ are 0.67 and 0.33 for the increase and the decrease, respectively, in $C_c$. It is apparent in Fig. 2-9 that the colloid-associated, solute and total radionuclide breakthroughs conform exactly to the predictions based on these values. The input parameters and 1-D model outputs for the cases of Figure 3-9 are provided in the electronic spreadsheet supplement to this report in the worksheet titled “Figure 3-9 Test Cases”.

## 3.4 Fourth Set of Test Cases: Hybrid Early Breakthrough and Reduced Retardation Behavior

One scenario that hasn't yet been discussed is a case where radionuclide adsorption to and desorption from colloids is slow enough relative to transport times that these reactions cannot be considered to be at equilibrium, yet the initial radionuclide association with colloids is large enough that the increase in early breakthrough concentrations of colloid-associated radionuclide approaches $C/C_0$ = 1 before a significant amount of solution-phase radionuclide breakthrough occurs. This situation corresponds to a hybrid of the early breakthrough cases of Section 3.1 and the reduced retardation cases of Section 3.3, showing some breakthrough characteristics of both sets of cases. Fig. 3-10 shows the results of two cases where the dimensionless colloid filtration rate constant, $\frac{SA}{V} k_{cs,ir} \tau$, is set to a low value of 0.01, which results in less colloid filtration than all earlier cases, and the steady-state colloid concentrations were set to $10^{-4}$ or $10^{-3}$ g/cm$^3$, respectively, which is much higher than in the cases of Section 3.1 ($10^{-6}$ g/cm$^3$). The input parameters and 1-D model outputs for the cases of Figure 3-10 are provided in the electronic spreadsheet supplement to this report in the worksheet titled "Figure 3-10 Test Cases".

Fig. 3-10 shows that the specified inputs for these cases result in both an early (conservative breakthrough fraction) of radionuclide, as well as an earlier approach to $C/C_0$ = 1 that is similar to the cases of Section 3.3. We note that the concentrations do not quite reach $C/C_0$ = 1 because of the retarding effect of the filtered colloids on the immobile surfaces at later times (even though the filtration rate constant was set to a low value, the high colloid concentrations in these simulations still result in a significant amount of colloid filtration). Additional discussion of these cases is provided in Reimus et al. (2016), Section 2.4.

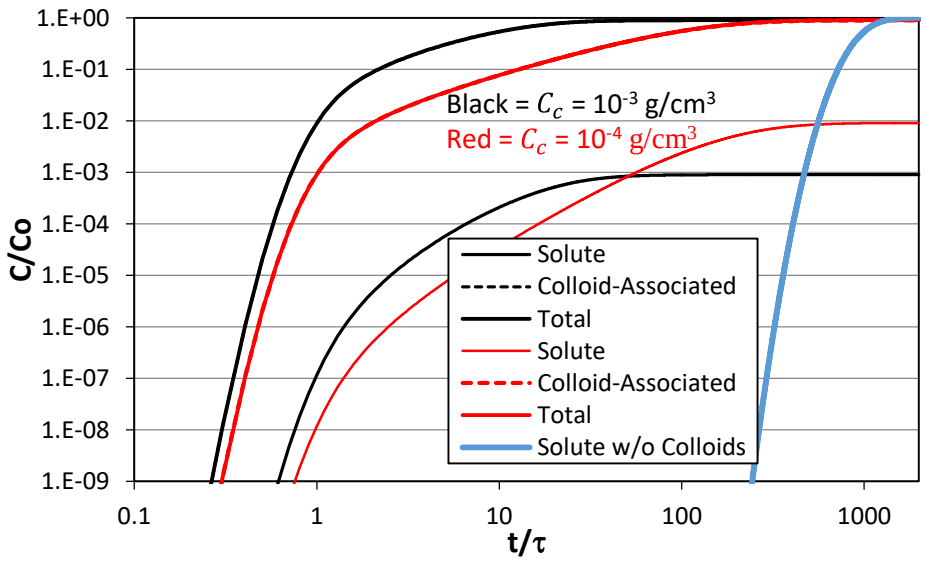


Figure 3-10. Solute, colloid-associated, and total breakthrough curves of a radionuclide assuming the model parameters of Fig. 3-1 except $\frac{SA}{V} k_{cs,ir} \tau$ = 0.01, $C_c$ = $10^{-4}$ g/cm$^3$ (red), $C_c$ = $10^{-3}$ g/cm$^3$ (black), which are 2 and 3 orders of magnitude greater than in Fig. 3-1. Both "colloid-associated" curves are obscured by the "total" curves. The blue curve is the radionuclide breakthrough in the absence of colloids.

## 3.5 Fifth Set of Test Cases: Reversible Filtration of Intrinsic Colloids

One final set of test cases focuses on the reversible filtration of colloids, as all previous test cases assumed only irreversible filtration. Reversible filtration will contribute to colloid-facilitated transport in situations where there is a very strong radionuclide association with colloids and the effective retardation factor of the colloids is less than the effective retardation factor of the solute in the absence of colloids. This situation is most closely aligned with the intrinsic colloid cases of Section 3.2. Fig. 3-11 shows the results of cases using the same input parameters as in Fig. 3-6 except $k_{ca}\tau$ = 0.01 and 1, respectively, and there is no irreversible colloid filtration, but reversible colloid filtration is defined using values of $\frac{SA}{V}k_{cs}\tau$ = 50 and $k_{sc}\tau$ = 5. Additionally, it is assumed that there is no production of colloids; i.e., $P_c$ = 0. These assumptions result in a deviation in the governing equations of the model from equations (3-1) through (3-6) because there must now be terms for filtration and resuspension of reversibly-filtered colloids, and the terms for irreversibly-filtered colloids and production of colloids disappear. We do not rewrite the new equations here because they are effectively captured in the general model of equations (2-1) through (2-8), and the differences from equations (3-1) through (3-6) should be readily apparent.

Figure 3-11 shows that the radionuclide breakthrough curves look qualitatively very much like the breakthrough curves in Fig. 3-6, except that the early arrival of the radionuclide is delayed by about a factor of 10 relative to the cases in Fig. 3-6. This delay occurs because all the colloids have an effective retardation factor of 10 as they move through the flow system, and the radionuclide cannot move any faster than the colloids. However, once the colloids break through, the strongly-associated radionuclides appear with them. The breakthrough concentration for the $k_{ca}\tau$ = 0.01 curve of Fig. 3-11 is about the same as in the $k_{ca}\tau$ = 0.1 case of Fig. 3-6 because the ten times slower desorption of the radionuclide from the colloids in Fig. 3-11 is countered by the 10 times longer residence time of the colloids in Fig. 3-11. The input parameters and 1-D model outputs for the cases of Figure 3-11 are provided in the electronic spreadsheet supplement to this report in the worksheet titled "Figure 3-11 Test Cases".

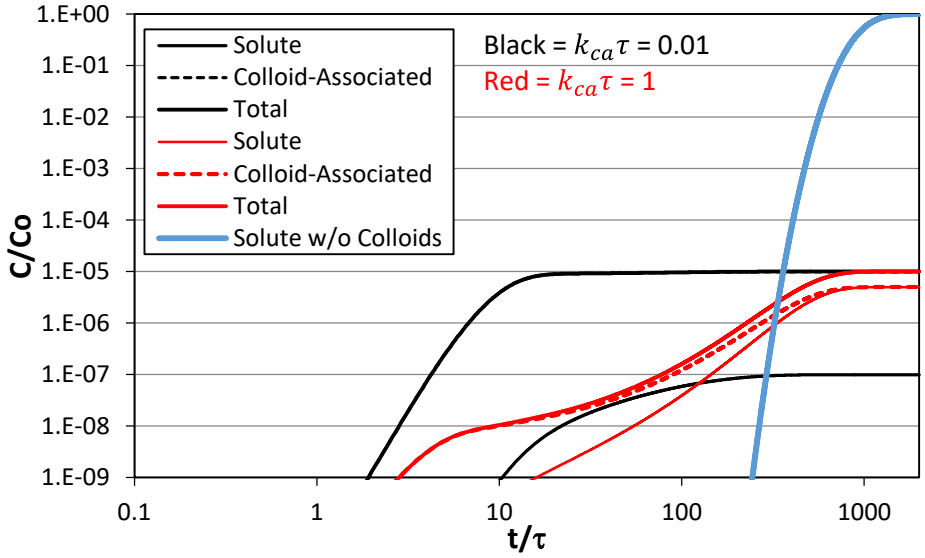


Figure 3-11. Solute, colloid-associated, and total breakthrough curves of a radionuclide assuming the model parameters of Fig. 3-6 except that $k_{ca}\tau$ = 0.01 (black) and 1 (red), and all colloid filtration is reversible with values of $\frac{SA}{V}k_{cs}\tau$ = 50 and $k_{sc}\tau$ = 5.

# 4. CONCLUSIONS

This report provides documentation of the mathematical basis for a colloid-facilitated radionuclide transport modeling capability that can be incorporated into GDSA-PFLOTRAN. It also provides numerous test cases against which the modeling capability can be benchmarked once the model is implemented numerically in GDSA-PFLOTRAN. The test cases were run using a 1-D numerical model developed by the author, and the inputs and outputs from the 1-D model are provided in the electronic spreadsheet supplement to this report so that all cases can be reproduced in GDSA-PFLOTRAN, and the outputs can be directly compared with the 1-D model. The cases include examples of all potential scenarios in which colloid-facilitated transport could result in the accelerated transport of a radionuclide relative to its transport in the absence of colloids (Sections 3.1 through 3.4). However, it cannot be claimed that the test cases of this report rigorously exercise all of the colloid-facilitated transport modeling capabilities that are documented in the mathematical basis because the test cases are limited to a single type of radionuclide adsorption site on both colloids and immobile surfaces and also to a single type of filtration site for colloids on immobile surfaces. Furthermore, the adsorption and filtration sites are assumed to be abundant enough that there are no capacity limitations for either adsorption or filtration. Additionally, only a single radionuclide and a single type of colloid are considered in the test cases, and all the cases are limited to 1-D transport with no diffusion of solutes into secondary (non-flowing) porosity. To include all these features would result in a staggering number of test cases, and many of these cases would end up testing model features that are of secondary importance to colloid-facilitated transport. The goal here was to test the features that matter the most for colloid-facilitated transport; i.e., slow desorption of radionuclides from colloids, slow filtration of colloids, and equilibrium radionuclide partitioning to colloids that is strongly favored over partitioning to immobile surfaces, resulting in a substantial fraction of radionuclide mass being associated with mobile colloids. One additional test case is provided in which the reversible filtration of colloids is exercised, as all other test cases assumed irreversible colloid filtration. Reversible filtration will contribute to colloid-facilitated transport in cases where there is a very strong radionuclide association with colloids and the effective retardation factor of the colloids is less than the effective retardation factor of the solute in the absence of colloids.

# 5. ACKNOWLEDGMENTS

This work was supported by the Spent Fuel and Waste Systems Technology Campaign of the Department of Energy's Fuel Cycle Research and Development Program. Los Alamos National Laboratory is managed and operated by Los Alamos National Security, LLC for the U.S. Department of Energy's National Nuclear Security Administration under contract DE-AC52-06NA25396.

# 6. REFERENCES

Reimus, P. W., Zavarin, M., and Wang, Y. 2016. *Colloid-Facilitated Radionuclide Transport: Current State of Knowledge from a Nuclear Waste Repository Risk Assessment Perspective*, FCRD-UFD-2016-000446, Fuel Cycle Research and Development Report, and LA-UR-16-26638, Los Alamos National Laboratory, Los Alamos, NM